

HiPreNets: High-Precision Neural Networks through Progressive Training

Ethan Mulle*, Wei Kang† and Qi Gong‡

June 19, 2025

Abstract

Deep neural networks are powerful tools for solving nonlinear problems in science and engineering, but training highly accurate models becomes challenging as problem complexity increases. Non-convex optimization and numerous hyperparameters to tune make performance improvement difficult, and traditional approaches often prioritize minimizing mean squared error (MSE) while overlooking L^∞ error, which is the critical focus in many applications. To address these challenges, we present a progressive framework for training and tuning high-precision neural networks (HiPreNets). Our approach refines a previously explored staged training technique for neural networks that improves an existing fully connected neural network by sequentially learning its prediction residuals using additional networks, leading to improved overall accuracy. We discuss how to take advantage of the structure of the residuals to guide the choice of loss function, number of parameters to use, and ways to introduce adaptive data sampling techniques. We validate our framework’s effectiveness through several benchmark problems.

1 Introduction

Fully-connected deep neural networks [26, 27, 15] have found widespread use in applications such as computer vision [18] and natural language processing [31, 24], yet they remain underutilized in scientific and engineering domains due to concerns about accuracy and safety [14]. Guaranteeing high accuracy on these problems is difficult because they are often high-dimensional and nonlinear. Much of the existing literature focuses on attaining a “good enough” average error rather than devoting significant effort to drive it closer to machine precision. Additionally, the final maximum error of a neural network approximation is generally ignored despite worst-case behavior being critical to analyze for sensitive applications [2].

For complex nonlinear, nonconvex problems, it can be hard to know if a neural network has converged to a high quality local minimum, let alone to the global minimum, when optimizing it [8, 10]. Once optimization reaches a local minimum or saddle point, escaping to a more optimal solution can be challenging. To do so often requires extensive hyperparameter tuning, which can be time consuming and does not guarantee improvement [5, 35, 28]. Understanding why certain hyperparameter configurations outperform others remains an open challenge. There is therefore generally no structured way of approaching the training and finetuning of a neural network.

One recent line of work explores improving neural network precision and interpretability through changes to model architecture [29, 16, 34, 13]. In particular, Kolmogorov–Arnold Networks (KANs) [19, 11] are a newly proposed architecture inspired by the Kolmogorov–Arnold representation theorem [17]. Instead of relying on compositions of simple, fixed nonlinearities (as in fully connected neural networks), KANs learn the nonlinearity itself through trainable 1D spline functions at each neuron. This gives them greater flexibility

*Department of Applied Mathematics, Baskin School of Engineering, University of California, Santa Cruz; emulle@ucsc.edu.

†Professor, Department of Applied Mathematics, Naval Postgraduate School. This work was supported in part by U.S. Naval Research Laboratory - Monterey, CA, the Air Force Office of Scientific Research, USA under Grant No.F4FGA03243G001, and the National Science Foundation (NSF), USA under Grant No.2202668.

‡Professor, Department of Applied Mathematics, Baskin School of Engineering, University of California, Santa Cruz. This work was supported in part by the National Science Foundation (NSF), USA under Grant No.2134235

and expressivity, particularly for problems with complicated low-dimensional structures. However, KANs introduce new challenges, such as higher memory requirements and the risk of overfitting if not properly regularized.

One classical machine learning approach for increasing the precision is gradient boosting [12, 7]. Gradient boosting is a machine learning technique used to improve the accuracy of predictions by combining multiple weak models into a stronger model. It does this sequentially, where each new model is trained to correct the errors made by the previous ones. Typically, this has been implemented in practice using decision trees [6, 22, 23], which are individually easy to understand and are low cost to optimize. However, they are prone to overfitting and their outputs are discontinuous and piecewise constant, which can make it difficult to apply them to complex real-world tasks [9].

In recent work, [4, 20] attempted to extend boosting to neural networks by proposing the idea of boosted neural networks. In these methods, fully connected neural networks are used as the “weak” models to be combined. These models are less interpretable and more costly to optimize than decision trees, but they are much better at capturing nonlinear patterns, can produce robust outputs, and can more easily be regularized to avoid overfitting. In [33], this approach was taken one step further by recognizing neural networks’ tendency to learn the low-frequency components of functions first, known as the spectral bias of neural networks [25]. As such, the low and high frequency parts of a dataset and the models’ residuals can be analyzed and incorporated into the boosting algorithm to further guide the training process. This analysis is insightful and was shown to work for low dimensional problems, but it appears much more difficult to apply it to higher dimensional problems. In summary, while these earlier works have applied boosting concepts to neural networks, they typically focused on shallow models or spectral insights that are hard to generalize in practice, and none of them analyze methods for reducing worst-case error.

To address these issues, we introduce a progressive training framework based on boosting in which the neural network is composed of multiple components trained sequentially. Each component has significantly lower complexity than the full network. This modularity of the framework also offers great flexibility by allowing for each component network to be trained with a different architecture and loss function that may better fit the data it encounters. By using a loss function and other training techniques at each iteration that incorporate information from the residuals, the training can be guided to preferentially reduce either the MSE or the maximum error.

We focus exclusively on applying the proposed techniques to regression problems, with accuracy measured by both mean squared error (MSE) and maximum error. While most neural network-based regression methods aim to minimize MSE, often by using it directly as the loss function [27], this approach is suitable only when reducing the average error across the dataset is sufficient. However, it falls short in applications where a single large error could lead to catastrophic failure (e.g., autonomous driving systems or medical diagnostics—see [1], [3]). Our proposed method integrates staged and normalized residual learning with architecture-adaptive modules and explicit L^∞ norm error mitigation strategies, enabling highly precise approximations critical in safety-sensitive applications.

In Section 2, we further develop the theory behind gradient boosted neural networks in a more structured way and highlight the resulting approximation error. We write out and test the algorithm on numerous regression examples, as well as investigate the impacts of the number of parameters used. We also compare our proposed method against KANs to understand the trade-offs between developing new methods that take advantage of existing architectures (our proposed method) versus developing completely new architectures (KANs) when trying to improve precision in machine learning. In Section 4 we examine how choice of loss function affects the performance of the technique on both RMSE and L^∞ norm error and evaluate it on our chosen examples. In Sections 5 and 6, we introduce the idea of weighted sampling and local patching and evaluate their performance. Finally, in Section 7, we present a boundary-aware training technique accomplished through domain expansion and then provide concluding remarks in Section 8. Overall, we validate the proposed method provides high precision results on a family of benchmark problems. The results demonstrate that the HiPreNet framework effectively improves accuracy measured by both MSE and maximum error. The code used is available at <https://github.com/etmulle/residual-training>.

2 High-Precision Neural Networks

One of the key advantages of our proposed HiPreNet framework is the breaking down of the haphazard training of a large neural network into the structured and targeted training of several small neural networks. Each of these neural networks will have its own associated loss function l and width h . Our framework progressively focuses on errors made by previous learners, enabling each new network to focus on correcting the mistakes of its predecessors. The training process is both simple and intuitive. Once a neural network has been trained and no longer shows significant improvement, we compute the residuals. These residuals are then normalized and used as targets for the next neural network in the sequence. The predictions of the new network are added to the original model’s outputs, yielding a more accurate overall prediction. This process can be repeated multiple times, producing a sequence of refinement networks, each one fine-tuning the ensemble’s performance by focusing on remaining errors. A diagram illustrating the training algorithm is given in Figure 1.

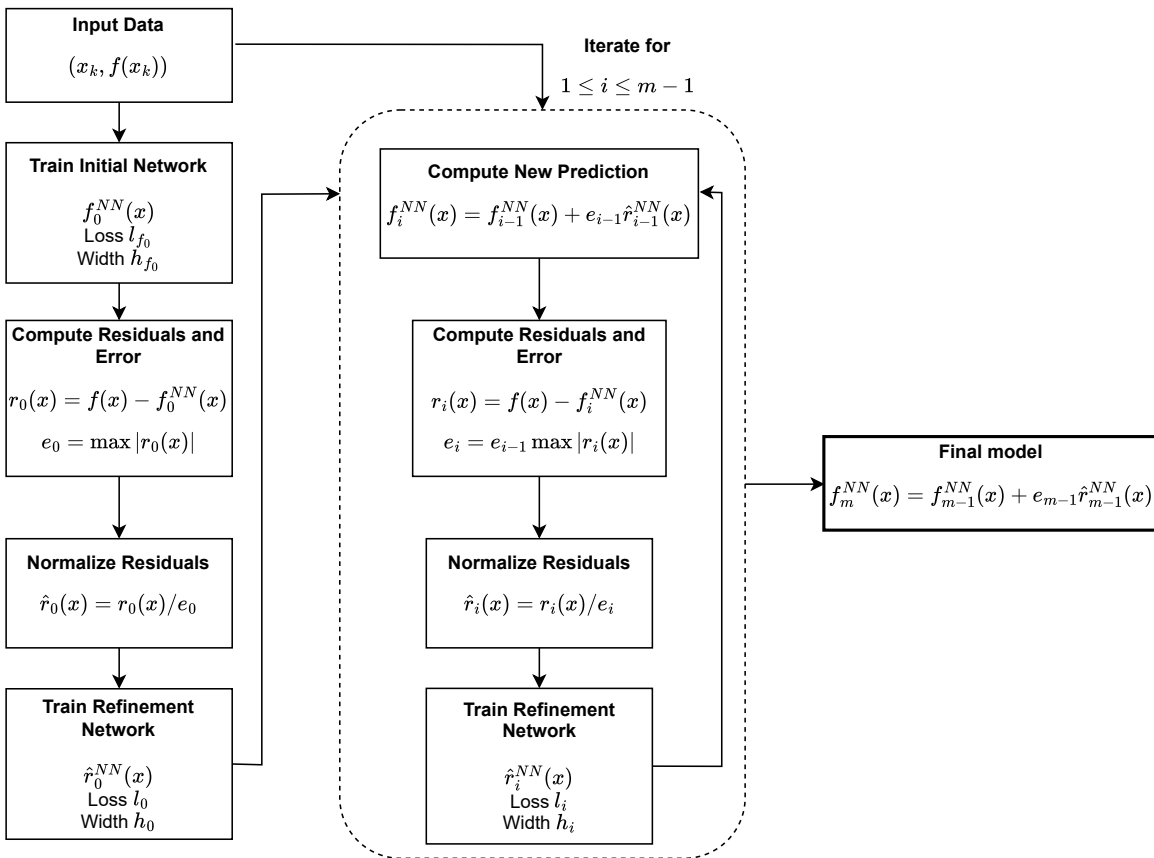


Figure 1: Illustration of the HiPreNet training process. Each component is trained sequentially and are combined to form the final model.

While the accuracy of an individual refinement network does still depend on chosen hyperparameters, the overall framework contributes significantly to performance gains by systematically addressing model weaknesses. In contrast, the performance of a single large network highly depends on extensive hyperparameter tuning, of which the optimal configuration can vary dramatically across different tasks, making the training process much less predictable. This decentralization of models also contributes to more manageable memory and computational demands, making the training process more accessible and scalable, especially in resource-constrained environments.

2.1 Algorithmic Formulation of HiPreNet Training

Let $f(x) : D \rightarrow R$ be a continuous function with a compact domain $D \subset R^n$. In this paper we are interested in approximating the unknown function $f(x)$ based on a given finite dataset of samples $\{(x_k, f(x_k))\}_{k=1}^N$. We will train a sequence of neural networks $f_i^{NN}(x)$, $i = 1, 2, \dots$, on this dataset to approximate the function and make a prediction for any $x \in D$, where the accuracy of the predictions will increase as i increases.

To assess the accuracy of the neural network approximation, we measure the discrepancy between $f(x)$ and its neural network approximation $f^{NN}(x)$ using the L^p norm over domain D :

$$\|f(x) - f^{NN}(x)\|_{L^p(D)}$$

We first choose $p = 2$, where the squared L^2 norm is defined as

$$\|f(x) - f^{NN}(x)\|_{L^2(D)}^2 = \int_D (f(x) - f^{NN}(x))^2 dx$$

As we only have a finite amount of samples of $(x, f(x))$, we approximate this integral by the sample average over the dataset and then take the square root to obtain the root mean squared error (RMSE)

$$RMSE = \sqrt{\frac{\sum_{i=1}^N (f(x_i) - f^{NN}(x_i))^2}{N}}$$

which converges to the true L_2 norm as $N \rightarrow \infty$.

We additionally consider the L^∞ norm defined as

$$\|f(x) - f^{NN}(x)\|_{L^\infty(D)} = \max_{x \in D} |f(x) - f^{NN}(x)|,$$

which is approximated by the maximum prediction error on the given dataset

$$\|f(x) - f^{NN}(x)\|_{L^\infty(D)} \approx \max_{1 \leq i \leq N} |f(x_i) - f^{NN}(x_i)|.$$

This metric allows us to evaluate the worst-case behavior of our trained neural network over the domain D .

Given a dataset $\{(x_k, f(x_k))\}_{k=1}^N$, we will design a neural network based model with high approximation accuracy through an progressive training process based on the residuals. Each neural network will be trained using loss function L , which, for regression problems, is typically chosen to be MSE loss:

$$L_{MSE} = \frac{\sum_{i=1}^N (f(x_i) - f^{NN}(x_i))^2}{N}$$

The process initiates with a neural network, $f_0^{NN}(x)$ to approximate $f(x)$. This initial network is usually of small size and low accuracy. Denote the initial approximation error e_0 as

$$e_0 = \|f(x) - f_0^{NN}(x)\|_{L^\infty}.$$

Next we introduce the residuals $r_0(x)$ and the normalized residuals $\hat{r}_0(x)$ as

$$r_0(x) = f(x) - f_0^{NN}(x), \quad \hat{r}_0(x) = \frac{r_0(x)}{e_0}.$$

Now, a new neural network, $\hat{r}_0^{NN}(x)$, can be trained to approximate $\hat{r}_0(x)$ with approximation error ϵ_0 such that

$$\|\hat{r}_0(x) - \hat{r}_0^{NN}(x)\|_\infty = \epsilon_0 < 1$$

This generates a new neural network approximation of function f as

$$f_1^{NN}(x) = f_0^{NN}(x) + e_0 \hat{r}_0^{NN}(x),$$

with an approximation error

$$\begin{aligned}
e_1 = \|f(x) - f_1^{NN}(x)\|_\infty &= \|f_0^{NN}(x) + r_0(x) - f_0^{NN}(x) - e_0 \hat{r}_0^{NN}(x)\|_\infty \\
&= \|e_0 \hat{r}_0(x) - e_0 \hat{r}_0^{NN}(x)\|_\infty \\
&= \epsilon_0 e_0 < e_0
\end{aligned}$$

Thus, the new approximation $f_1^{NN}(x)$ is more accurate than the initial neural network approximation $f_0^{NN}(x)$.

Repeating this process we can generate a sequence of increasingly accurate neural network approximations of $f(x)$ as

$$f_{i+1}^{NN}(x) = f_i^{NN}(x) + e_i \hat{r}_i^{NN}(x),$$

where $e_i = \|f(x) - f_i^{NN}(x)\|_\infty$ is the previous approximation error and \hat{r}_i^{NN} is a newly trained neural network that approximates, \hat{r}_i , the normalized residual from the previous step, i.e.,

$$\hat{r}_i^{NN} \approx \hat{r}_i(x) = \frac{f(x) - f_i^{NN}(x)}{e_i}.$$

Suppose \hat{r}_i^{NN} is accurate enough so that

$$\|\hat{r}_i(x) - \hat{r}_i^{NN}(x)\|_\infty = \epsilon_i < 1.$$

Then, we have

$$\begin{aligned}
e_{i+1} = \|f(x) - f_{i+1}^{NN}(x)\|_\infty &= \|f_i^{NN}(x) + e_i \hat{r}_i(x) - f_i^{NN}(x) - e_i \hat{r}_i^{NN}(x)\|_\infty \\
&= \|e_i \hat{r}_i(x) - e_i \hat{r}_i^{NN}(x)\|_\infty \\
&= \epsilon_i e_i < e_i
\end{aligned}$$

Thus, the accuracy of the new approximation model $f_{i+1}^{NN}(x)$ keeps increasing with the number of iterations, provided the first neural network approximates the original function with error $e_0 < 1$ and that each residual neural network approximates the normalized residuals with error $\epsilon_i < 1$. Supposing we have m total refinement networks, this gives a final approximation $f(x)$ as

$$f(x) \approx f_m^{NN}(x) = f_0^{NN}(x) + \sum_{i=0}^{m-1} e_i \hat{r}_i^{NN}(x)$$

which is the sum of the outputs of all of the trained model. This is visualized in the diagram given in Figure 2.

In practice, several factors can cause the condition of the approximation error of each network to be smaller than one to not be met. Firstly, the residuals may exhibit high-frequency, non-smooth behavior that is hard to approximate with standard architectures, meaning insufficient model capacity in deeper stages may limit residual learning. Additionally, as residuals become increasingly small and oscillatory, numerical precision and optimizer stability may also limit practical convergence. Furthermore, noisy training data or very limited sampling may degrade the estimated residual accuracy, which we do not investigate in this work. In all these cases, the reduction of L^∞ norm error may stall or reverse. While we do observe convergence empirically in all of our experiments, formal guarantees remain an open area for future work. The pseudocode of the algorithm is given in Algorithm 1.

Remark 1 *The total size of the model depends directly on the size of the neural networks used in each training iteration. Additionally, the architecture of the network used in each iteration does not have to remain fixed; the loss function, activation function, and number of layers and neurons used in the first iteration can be completely different from those used for the last iteration. This allows for increased adaptability to what is observed in the residuals, where different architectures may be better suited for different residual patterns.*

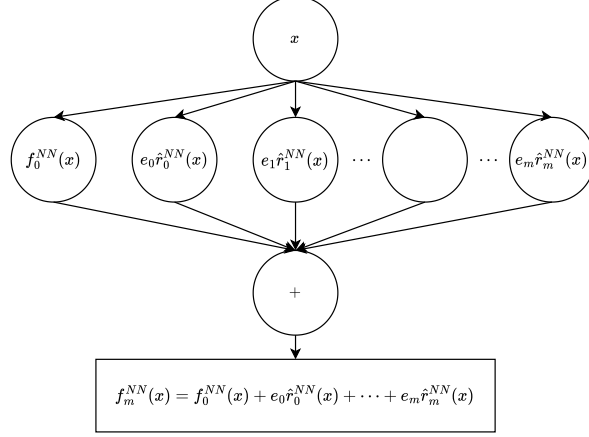


Figure 2: Illustration of making inferences with the trained model. The same input x is the input to all of the trained networks, where their outputs are summed together to obtain the final prediction $f_m^{NN}(x)$.

Algorithm 1 HiPreNet Training Algorithm

Require: Dataset $(\mathbf{x}, \mathbf{f}) = \{(x_k, f(x_k))\}_{k=1}^N$, trained neural network f_0^{NN} , tolerance tol

$error \leftarrow L(\mathbf{f}, f_0^{NN}(\mathbf{x}))$

$r_0 \leftarrow \mathbf{f} - f_0^{NN}(\mathbf{x})$

$e_0 \leftarrow \max |r_0|$

\triangleright estimate of true e_0

$\hat{r}_0(\mathbf{x}) \leftarrow \frac{r_0}{e_0}$

$\hat{r}_0^{NN}(\mathbf{x}) \leftarrow train(\mathbf{x}, \hat{r}_0(\mathbf{x}))$

$i \leftarrow 1$

while $error > tol$ **do**

$f_i^{NN}(\mathbf{x}) \leftarrow f_{i-1}^{NN}(\mathbf{x}) + e_i \hat{r}_i^{NN}(\mathbf{x})$

$r_i(\mathbf{x}) \leftarrow \mathbf{f} - f_i^{NN}(\mathbf{x})$

$e_i \leftarrow e_{i-1} \cdot \max |r_i(\mathbf{x})|$

\triangleright estimate of true e_i

$\hat{r}_i(\mathbf{x}) \leftarrow \frac{r_i(\mathbf{x})}{e_i}$

$\hat{r}_i^{NN}(\mathbf{x}) \leftarrow train(\mathbf{x}, \hat{r}_i(\mathbf{x}))$

$error \leftarrow L(\mathbf{f}, f_i^{NN}(\mathbf{x}))$

$i \leftarrow i + 1$

end while

Remark 2 It is important to note that the true approximation error e_i cannot be obtained in practice, as it is defined using the L^∞ norm and we can only train the neural networks on a limited dataset. As such, in our algorithm, we estimate e_0 from residuals r_0 as

$$e_0 \approx \max |r_0|$$

and each e_i from residuals r_i as

$$e_i \approx e_{i-1} \cdot \max |r_i(\mathbf{x})|$$

2.2 Preliminary Experiments on a Benchmark Function

Throughout the following sections, we test our algorithm on five different functions from the Feynman dataset first introduced in [30]. Each function is numbered and corresponds to a different dimensionless multi-variable function. These functions correspond to well known physical laws and relations. The functions are written out in Table 1 with their number in the dataset and both their original and dimensionless forms. For this paper, we attempt to learn the dimensionless forms of the functions. The dataset contains 1,000,000 samples for each function, which were all used for training the networks. To test the networks, we randomly generate an additional 1,000,000 validation samples for each function with each variable in the domains given in [30].

Number	Function	Dimensionless Function	Dimensionality
I.6.2	$f(\theta, \sigma) = \exp(-\frac{\theta^2}{2\sigma^2})/\sqrt{2\pi\sigma^2}$	$f(\theta, \sigma) = \exp(-\frac{\theta^2}{2\sigma^2})/\sqrt{2\pi\sigma^2}$	2
I.9.18	$f(G, \mathbf{m}, \mathbf{x}, \mathbf{y}, \mathbf{z}) = \frac{Gm_1m_2}{(x_2-x_1)^2+(y_2-y_1)^2+(z_2-z_1)^2}$	$f(a, b, c, d, e, f) = \frac{a}{(b-1)^2+(c-d)^2+(e-f)^2}$	6
I.13.12	$f(G, m_1, m_2, r_1, r_2) = Gm_1m_2(\frac{1}{r_2} - \frac{1}{r_1})$	$f(a, b) = a(\frac{1}{b} - 1)$	2
I.26.2	$f(n, \theta_2) = \arcsin(n \sin \theta_2)$	$f(n, \theta_2) = \arcsin(n \sin \theta_2)$	2
I.29.16	$f(x_1, x_2, \theta_1, \theta_2) = \frac{1}{\sqrt{x_1^2 + x_2^2 - 2x_1x_2 \cos(\theta_1 - \theta_2)}}$	$f(a, \theta_1, \theta_2) = \frac{1}{\sqrt{1 + a^2 - 2a \cos(\theta_1 - \theta_2)}}$	3

Table 1: The selected functions from the Feynman dataset with their dimensionless forms.

To begin with, we first compare our algorithm’s performance on Function I.13.12 with the performance of a single standard fully connected network with the same number of parameters, but made wider (going from 5 to 11 neurons in each hidden layer) or deeper (going from 5 to 19 hidden layers of 5 neurons each). For our algorithm, an initial predictor neural network as well as three refinement networks were initialized and trained. All networks contain five hidden layers with five neurons each and use tanh as their activation function.

Each refinement network is optimized with SciPy’s [32] Broyden–Fletcher–Goldfarb–Shanno (BFGS) algorithm [21] for a maximum of 25000 iterations, using a gradient tolerance of 1e-12. The wide and deep fully connected networks are optimized with BFGS for a maximum of 100000 iterations. We use BFGS for training each network due to its strong local convergence properties and robustness in high precision settings. As a quasi-Newton method, BFGS leverages curvature information to guide updates more effectively than first-order methods, enabling more reliable convergence to low error solutions. While computationally more intensive due to requiring more memory and compute time, its performance is well-suited to the relatively small networks used in our framework, making it an ideal choice for achieving the extremely low errors targeted in this work.

We compare the lowest RMSE over three independent trials, solely changing the random seed. As shown in Table 2, the HiPreNet approach achieves a lower RMSE than either of the traditional fully connected neural network approaches.

Method	Validation RMSE	Parameters per Training	Size of Model
Wider FCNN	6.851e-06	573	573
Deeper FCNN	1.485e-04	561	561
HiPreNet	2.611e-06	141	564

Table 2: RMSE for Function I.13.12 using a fully connected network with 5 hidden layers with 11 neurons each (wider), 19 hidden layers with 5 neurons each (deeper), and the described HiPreNet setup with four fully connected networks which each have 5 hidden layers of 5 neurons each,

2.3 Comparison with Kolmogorov–Arnold Networks (KANs)

It is admittedly not difficult to beat an untuned fully connected network in performance, so we also compare our results to the results obtained by the Kolmogorov-Arnold networks (KANs) and fully connected networks presented in [19], which are evaluated on the same Feynman dataset. As previously mentioned, instead of having fixed activation functions like standard fully connected networks, KANs learn the nonlinearities themselves through trainable 1D spline functions at each neuron.

For each dataset, an initial predictor neural network as well as three refinement networks were initialized and trained. All networks contain five hidden layers with five neurons each and use tanh as their activation function. Each network was trained using BFGS as the optimizer with 25000 maximum iterations. We run each simulation for three different random seeds and report the results for the seed that provided the lowest validation error.

The initial RMSE and final RMSE after the training the HiPreNets are compared to each other for the different validation datasets in Table 3. We also compare the number of parameters needed for each model. As previously mentioned, in training a HiPreNet, multiple neural networks are trained sequentially and are then combined to create a final model for inference. In Table 3, the “Parameters per Training” column indicates the number of parameters in each individual neural network, while the “Total Model Size” column indicates the total number of parameters in the final model. It is not precisely clear the exact number of parameters used in each KAN from [19], so we report an estimate based on the authors’ presented figures in the “KAN Model Size” column in Table 3.

The change in RMSE as more refinement networks are trained is visualized in Figure 3(a). In all cases, each refinement network successively reduces the error. By the addition of the final refinement network, the final RMSE obtained is lower than the best reported RMSE in [19]. For Function I.6.2 in particular, by the addition of the final refinement network, the MSE ($1.832e-08$ RMSE = $3.356e-16$ MSE) has reached near machine epsilon ($2.220e-16$) for 64-bit double precision.

Function	Initial RMSE	Final RMSE	KAN RMSE	Parameters per Training	Total Model Size	KAN Model Size
I.6.2	4.262e-06	1.832e-08	2.86e-05	141	564	$\mathcal{O}(10^2)$
I.9.18	4.712e-04	5.801e-05	1.48e-03	161	644	$\mathcal{O}(10^2)$
I.13.12	3.403e-05	2.611e-06	1.42e-03	141	564	$\mathcal{O}(10^2)$
I.26.2	3.821e-04	8.076e-05	7.90e-04	141	564	$\mathcal{O}(10^2)$
I.29.16	6.528e-04	1.811e-04	3.20e-03	146	584	$\mathcal{O}(10^2)$

Table 3: Comparison of RMSE achieved by HiPreNets and Kolmogorov–Arnold Networks (KANs) across selected functions. Parameter count per each model training and total model sizes are also listed.

2.4 Empirical Insights from Early Experiments

The previous results have demonstrated that the HiPreNet framework provides a structured way of reducing the RMSE on a set of problems as compared to both traditional approaches of using fully connected neural networks and more recent KANs. To further understand the advantages and disadvantages of the HiPreNet

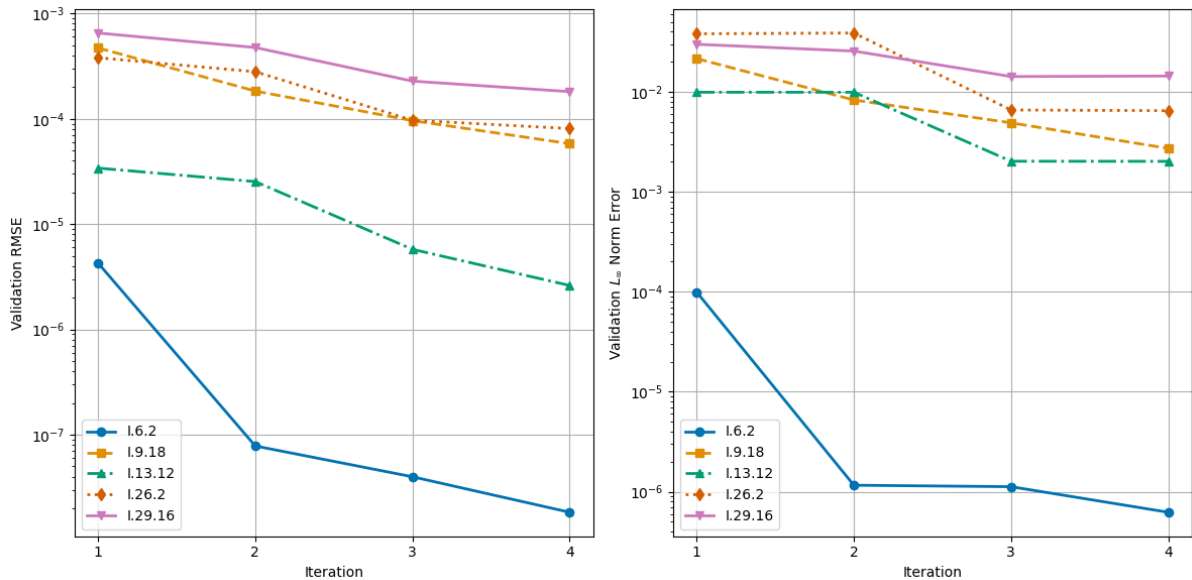


Figure 3: (a) RMSE progression across HiPreNet stages. (b) L^∞ norm error progression across HiPreNet stages. Model 1 is the initial network and each subsequent model learns to approximate the residuals of the previous model.

framework, we first report the L^∞ norm error on the five chosen Feynman functions in Table 4. We also show the change in L^∞ norm error as more refinement networks are trained in Figure 3(b). As previously mentioned, the L^∞ norm error is a valuable metric for quantifying the worst-case behavior of a model, as opposed to RMSE which quantifies the average behavior of a model. Analyzing this behavior is critical for applications such as healthcare, where a catastrophic single error can have enormous real-world consequences. Although there is a reduction in L^∞ norm error by the time the final refinement network is added, it is less noticeable than the reduction in RMSE.

Function	Initial L^∞ Norm	Final L^∞ Norm
I.6.2	9.948e-05	6.221e-07
I.9.18	2.157e-02	2.722e-03
I.13.12	9.941e-03	2.021e-03
I.26.2	3.822e-02	6.527e-03
I.29.16	3.000e-02	1.443e-02

Table 4: Initial and final L^∞ norm errors for each function, showing the change resulting from training a HiPreNet.

We also further illustrate the results for Function I.6.2, though the following observation holds true for all of the functions in Table 1. In Figure 4 we show plots of the true function, the final approximation after training a HiPreNet, and the final residuals. In Figure 5, we show surface and contour plots of the residuals at each stage of the training process. Each successive network generally succeeds in approximating the residuals of its predecessor on average, but has difficulty in capturing the more local, oscillatory and high frequency behavior that emerges with the later residuals, often along the boundary of the dataset. This indicates that the later networks may not be powerful enough to precisely capture this more complex behavior. When this is combined with the choice of MSE loss which focuses on reduction of the average error, there is little incentivizing a decrease in the L^∞ norm error.

Therefore, while the HiPreNet algorithm has already shown to be a viable method for reducing RMSE in a structured way, there are three key takeaways of this initial approach that we take note of and will

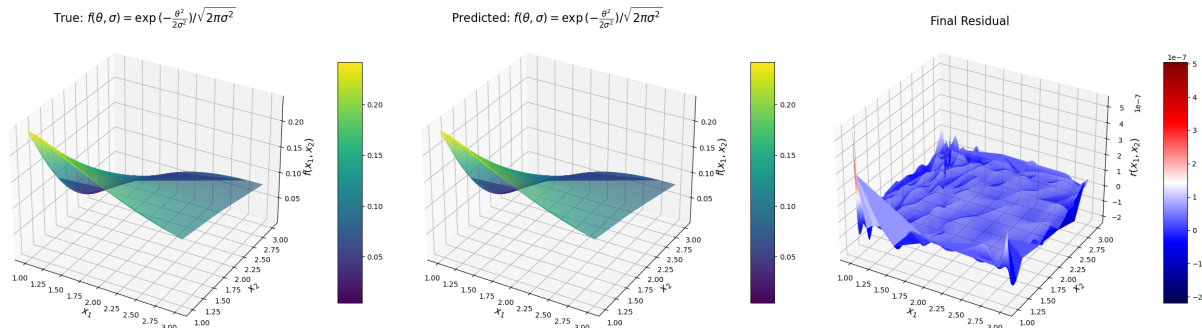


Figure 4: Visual comparison of the true function for Function I.6.2, the final model approximation, and the remaining residuals after training.

investigate in the coming sections to further improve the algorithm:

1. The residual functions become more oscillatory as more networks are added. Early residuals show coarse, low frequency errors, while later residuals often display more localized and higher frequency behavior and are therefore more difficult to learn. Knowing this, how many parameters are needed in each successive network?
2. Using mean squared error as the loss function for the refinement networks does reduce the average error, but is less ideal for reducing the maximum (L^∞ norm) error. Is there a better loss function that can be used to prioritize reducing the L^∞ norm error?
3. Before training each network, we can analyze the residuals to observe any regions that are difficult to learn. Can we modify the HiPreNet algorithm to take advantage of this information?

3 Network Width Adaptation in Residual Stages

From classical neural network theory it is known that as the width of a fully connected neural network increases, the complexity of the behavior that it can capture grows. As we have observed that the complexity of the residuals grow as more iterations of the HiPreNet algorithm happen, this indicates that the width of the refinement networks should be consistently increased to match this.

An empirical observation throughout our experiments is that the residual functions at each stage tend to become increasingly oscillatory, often exhibiting a greater number of local extrema. This suggests that the complexity of the residuals grows with each iteration, possibly in a linear fashion. One potential heuristic for determining the width of successive refinement networks is to match the network capacity to the number of extrema or local variations in the residuals. While we adopt a linearly increasing width schedule in this work, a more principled approach remains an open area for future investigation.

To confirm that this idea improves the HiPreNet framework, we fix the initial neural network and three residual neural networks to all have a depth of five hidden layers. We then vary the width of the layers for each network to be [5-5-5-5], [20-20-20-20], and [5-10-15-20]. For example, for the [5-10-15-20] case, the initial network will have 5 neurons in each layer, the first refinement network will have 10 neurons in each layer, the second refinement network will have 15, and the third refinement network will have 20. This allows for each additional network to have more capacity to fit the increasingly complex residual structures.

The results are summarized in Table 5 and plotted in Figure 6. We first observe that for the HiPreNet approach, there is a significant reduction in RMSE and generally a smaller reduction in L^∞ norm error (with the exception of Function I.26.2) when moving from a [5-5-5-5] setup to [5-10-15-20], corresponding to

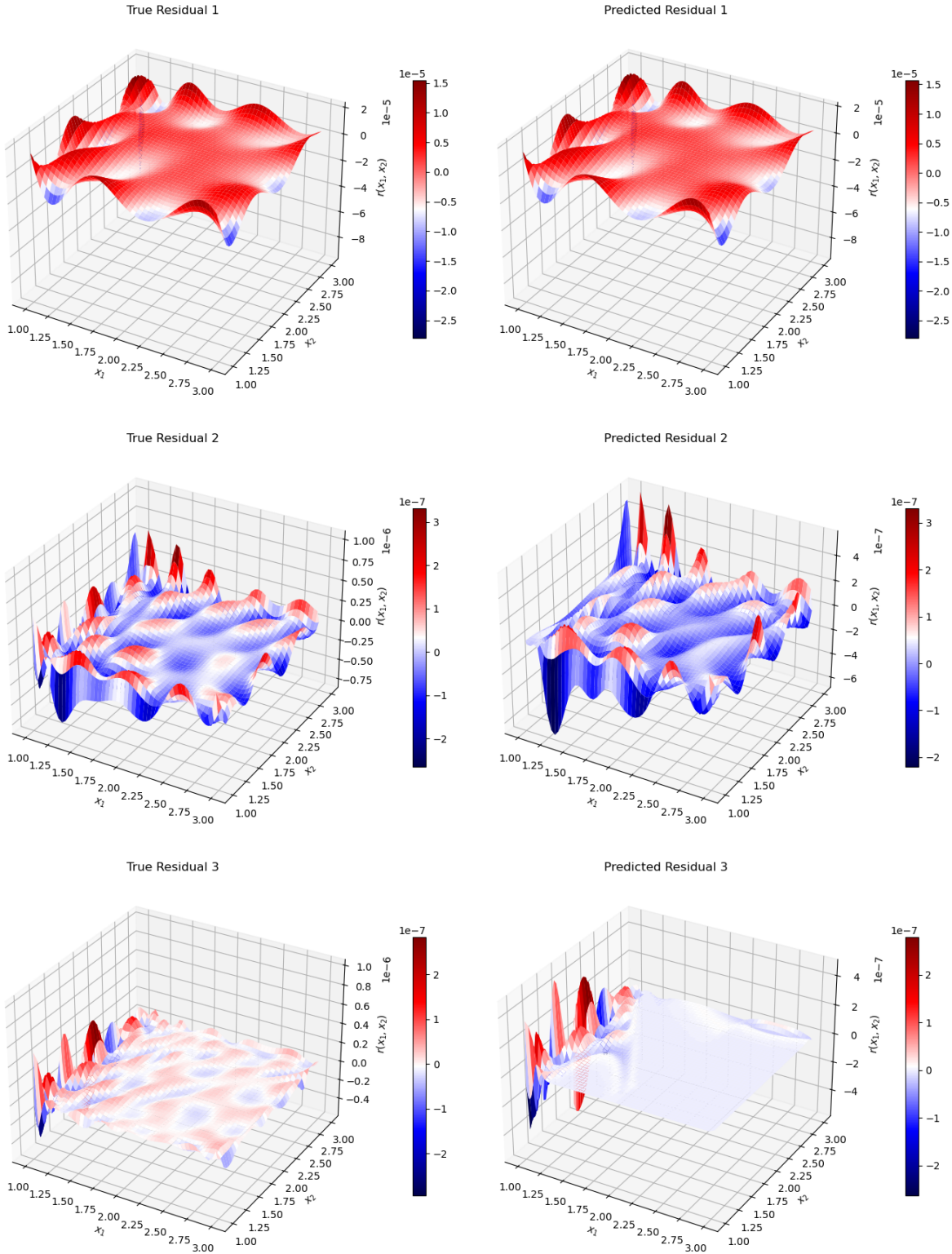


Figure 5: Surface plots of the residuals from each stage of the HiPreNet training process for Function I.6.2. Note that the axis and colorbar scales between neighboring plots may differ to accurately illustrate the loss landscape from each approach.

roughly a sixfold increase in the total number of parameters. A comparison of the residuals at each iteration when using [5-5-5-5] versus [5-10-15-20] is shown in Figure 7.

Function	Network Structure	Final RMSE	Final L^∞ Norm Error	Parameters per Training	Model Size
I.6.2	5-5-5-5	1.832e-08	6.221e-07	141	564
	20-20-20-20	2.204e-12	1.987e-10	1761	7044
	5-10-15-20	1.688e-11	1.341e-09	141, 481, 1021, 1761	3404
I.9.18	5-5-5-5	5.801e-05	2.722e-03	161	644
	20-20-20-20	1.324e-07	1.194e-04	1841	7364
	5-10-15-20	1.535e-07	9.822e-05	161, 521, 1081, 1841	3604
I.13.12	5-5-5-5	3.679e-06	2.021e-03	141	564
	20-20-20-20	1.789e-07	1.510e-04	1761	7044
	5-10-15-20	2.171e-07	1.501e-04	141, 481, 1021, 1761	3404
I.26.2	5-5-5-5	8.076e-05	6.527e-03	141	564
	20-20-20-20	3.156e-05	1.214e-02	1761	7044
	5-10-15-20	2.977e-05	1.495e-02	141, 481, 1021, 1761	3404
I.29.16	5-5-5-5	1.811e-04	1.443e-02	146	584
	20-20-20-20	1.056e-05	2.040e-03	1781	7124
	5-10-15-20	1.239e-05	1.461e-03	146, 491, 1036, 1781	3454

Table 5: Summary of RMSE, L^∞ norm error, parameters used for training each network, and total model size across different neuron configurations used in the refinement networks for each function.

One might also expect that simply making each network bigger will lead to a reduction in loss. However, increasing the setup further from [5-10-15-20] to [20-20-20-20], which approximately doubles the parameter count, yields minimal improvement in both RMSE and L^∞ norm error. This suggests that simply setting all widths to the same value is less efficient than gradually increasing them. Moreover, in the [20-20-20-20] case, the later networks may struggle to capture the complex residual behavior from their preceding network, indicating that a schedule like [20-25-30-35] might be needed. However, this quickly becomes computationally infeasible, requiring increasingly more memory and compute time especially if using BFGS as the optimizer. Overall, gradually widening the refinement networks proves to be a more effective strategy for balancing computational cost with model expressiveness, and careful design of the number of parameters in each neural network provides an important avenue for enhancing final model performance.

4 Loss Function Design for L^∞ Norm Error Reduction

As previously discussed, when using mean-squared error as the loss function for the refinement networks, the L^∞ error may remain constant or even increase despite the mean-squared error consistently decreasing. This is often due to sharp peaks in the residuals, which are typically located near the boundaries of the input domain. Using MSE as the loss function may cause the refinement networks to ignore these extreme, but very localized deviations in favor of focusing on areas which better reduce the mean error.

Direct optimization of the L^∞ norm is difficult, as it is non-differentiable and highly sensitive to single-point fluctuations, which complicates the training dynamics of neural networks. Moreover, relatively little prior work has focused on developing loss functions that specifically aim to minimize the L^∞ error. One way we attempt to focus the refinement networks on reducing the L^∞ norm error is by using a weighted

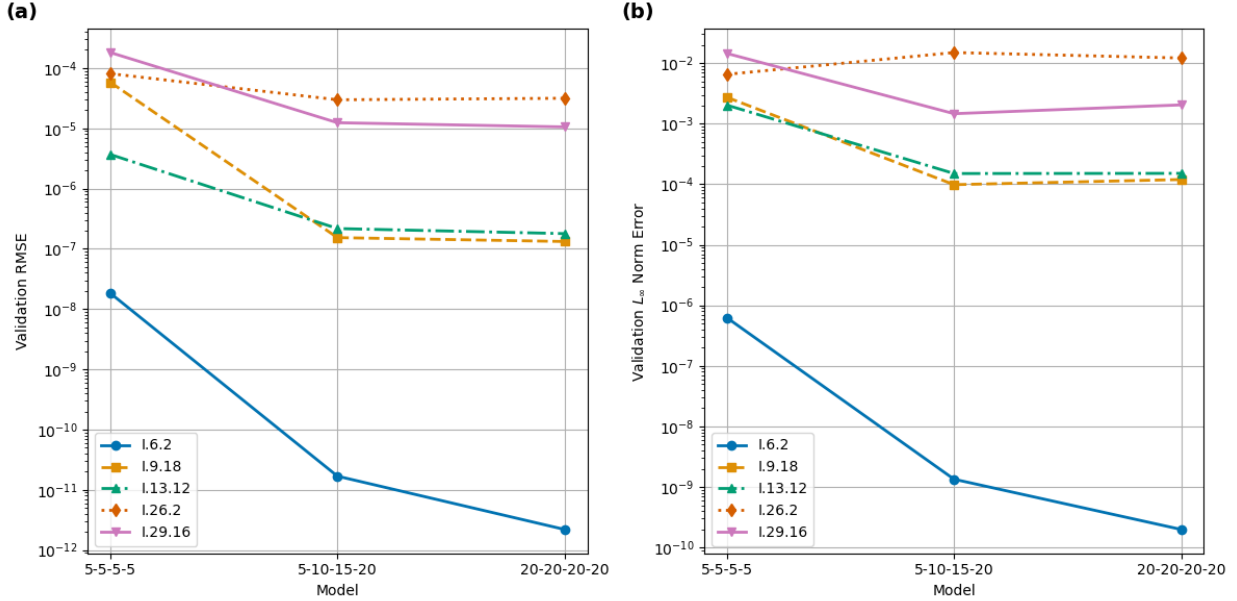


Figure 6: Impact of varying neuron counts in successive refinement networks on model validation RMSE and L^∞ norm error for all functions.

mean-squared error (WMSE) loss function. If at iteration i we are training refinement network \hat{r}_i^{NN} to approximate the residual \hat{r}_i , the WMSE loss function is defined as

$$WMSE = \frac{\sum_{k=1}^N w_k (\hat{r}_i(x_k) - \hat{r}_i^{NN}(x_k))^2}{N}$$

where

$$w_k = (1 + |\hat{r}_i(x_k)|)$$

Note that for this approach, the loss function used to train initial network f_0^{NN} remains as MSE loss.

This choice of weighting term increases the importance of accurately fitting regions where the target function exhibits large magnitudes, which in the case of the refinement networks, corresponds to peaks in the target residuals. By emphasizing these high-magnitude regions, the refinement networks are encouraged to reduce errors where they matter most for controlling the L^∞ norm.

We evaluate each function in Table 1 using a HiPreNet configuration with four stages and network widths [5–10–15–20], employing the tanh activation function and BFGS as the optimizer. For the refinement networks, we compare using the two different loss functions to train them: mean squared error (MSE) and weighted mean squared error (WMSE). The resulting test RMSE and L^∞ norm errors are reported in Table 6.

Figure 8 shows the validation error from each network in the HiPreNet training process first when MSE is used as the loss function, and then when WMSE is used as the loss function. We observe that WMSE can achieve a lower L^∞ norm error and even a lower RMSE than standard MSE loss, although the better choice between the two loss functions appears highly problem dependent.

For Function I.29.16 and I.13.12, using WMSE led to worse performance in both RMSE and L^∞ norm error compared to standard MSE. This suggests that WMSE may overfit to regions that contain a small subset of data points with large weights. In such cases, the weighting scheme can misdirect learning capacity if residuals exhibit erratic or noisy behavior, causing the model to struggle to generalize. Moreover, as mentioned previously, the L^∞ norm itself is inherently challenging to optimize due to its non-differentiability and sensitivity to outliers. WMSE serves as a proxy to mitigate this, but it cannot fully replicate direct L^∞ norm minimization.

Equation I.6.2

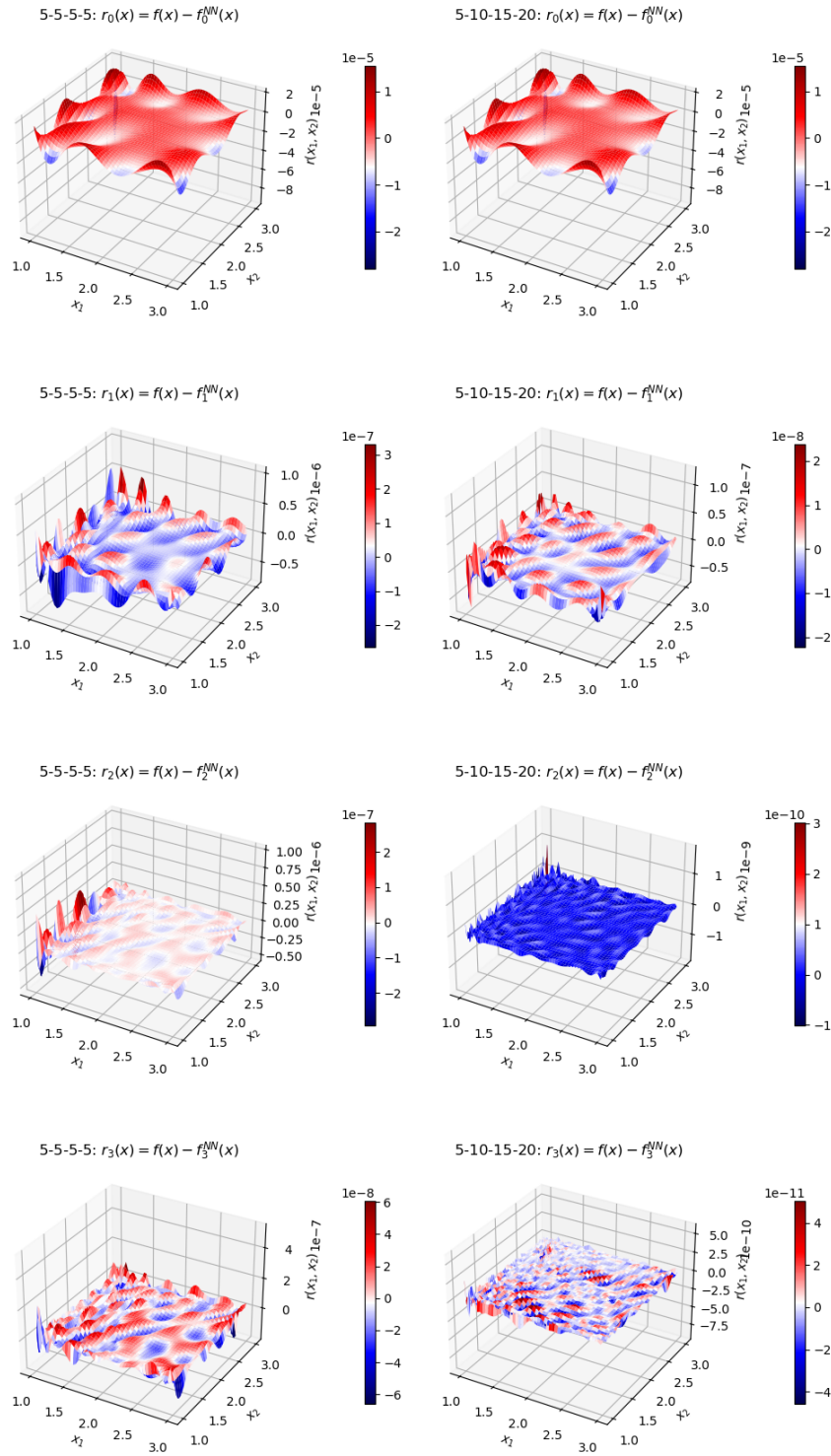


Figure 7: Residuals at each training stage for Function I.6.2 using a [5-5-5-5] and [5-10-15-20] network configuration. Note that the axis and colorbar scales between neighboring plots may differ to accurately illustrate the loss landscape from each approach.

Function	Loss Function	Final RMSE	Final L^∞ Norm Error
I.6.2	MSE	1.688e-11	1.341e-09
	WMSE	9.520e-12	5.298e-10
I.9.18	MSE	1.535e-07	9.822e-05
	WMSE	5.377e-07	3.732e-05
I.13.12	MSE	2.850e-07	1.585e-04
	WMSE	6.017e-07	4.532e-04
I.26.2	MSE	2.977e-05	1.495e-02
	WMSE	2.028e-05	8.061e-03
I.29.16	MSE	1.239e-05	1.461e-03
	WMSE	5.138e-05	2.508e-03

Table 6: Final RMSE and L^∞ norm error for each function using MSE and WMSE loss functions in the HiPreNet framework.

In summary, while WMSE can be beneficial for reducing worst-case error, it is not a universally superior choice. Selection of loss function should depend on the application’s tolerance for average versus maximum error, with WMSE loss potentially being better for one or both metrics depending on the details of the problem.

5 Weighted Sampling Based on Residual Errors

Even after the seemingly successful training of a neural network, certain regions of the input domain can remain poorly approximated, particularly near domain boundaries or in areas with sharp gradients. To address this, we introduce strategies that refine the training dataset based on a model’s error distribution. By prioritizing regions with large residuals, networks can focus their learning on where it is most needed, improving both global accuracy and worst-case error.

To further improve the performance of HiPreNet training, we introduce a weighted sampling strategy that leverages information from the current residuals to adaptively guide the training of subsequent networks. Rather than treating all training points equally, we assign greater sampling priority to data points with higher residual error, ensuring that regions with poor approximation are more strongly emphasized in future training. No new data is generated for this approach, it is a resampling of the existing training data.

Let the residual at iteration i be defined as

$$r_i(x) = f(x) - f^{NN}(x) - \sum_{j=0}^{i-1} e_j \hat{r}_j^{NN}(x)$$

which is then normalized as

$$\hat{r}_i(x) = \frac{r_i(x)}{e_i}$$

Given a discrete set of training samples $\mathbf{x} = \{x_1, x_2, \dots, x_N\}$, we define a sampling probability p_k at each iteration i for each training sample $x_k \in \mathbf{x}$ where

$$(p_k)_i = \frac{|\hat{r}_i(x_k)|}{\sum_{j=1}^N |\hat{r}_i(x_j)|}, \quad \text{for } k = 1, 2, \dots, N$$

to form a discrete probability distribution over the dataset. We use this distribution to resample the training dataset, giving higher selection probability to data points with larger residual error. Each refinement network is now trained on a subset $(x_{sampled}, \hat{r}_i(x_{sampled}))$ of the original data drawn according to $(p_k)_i$ which incentivizes it to concentrate on high error regions.

This approach is implemented by computing the residuals after each refinement network stage, converting them to sampling probabilities, and drawing a new batch of training samples accordingly. Importantly, this

Equation I.6.2

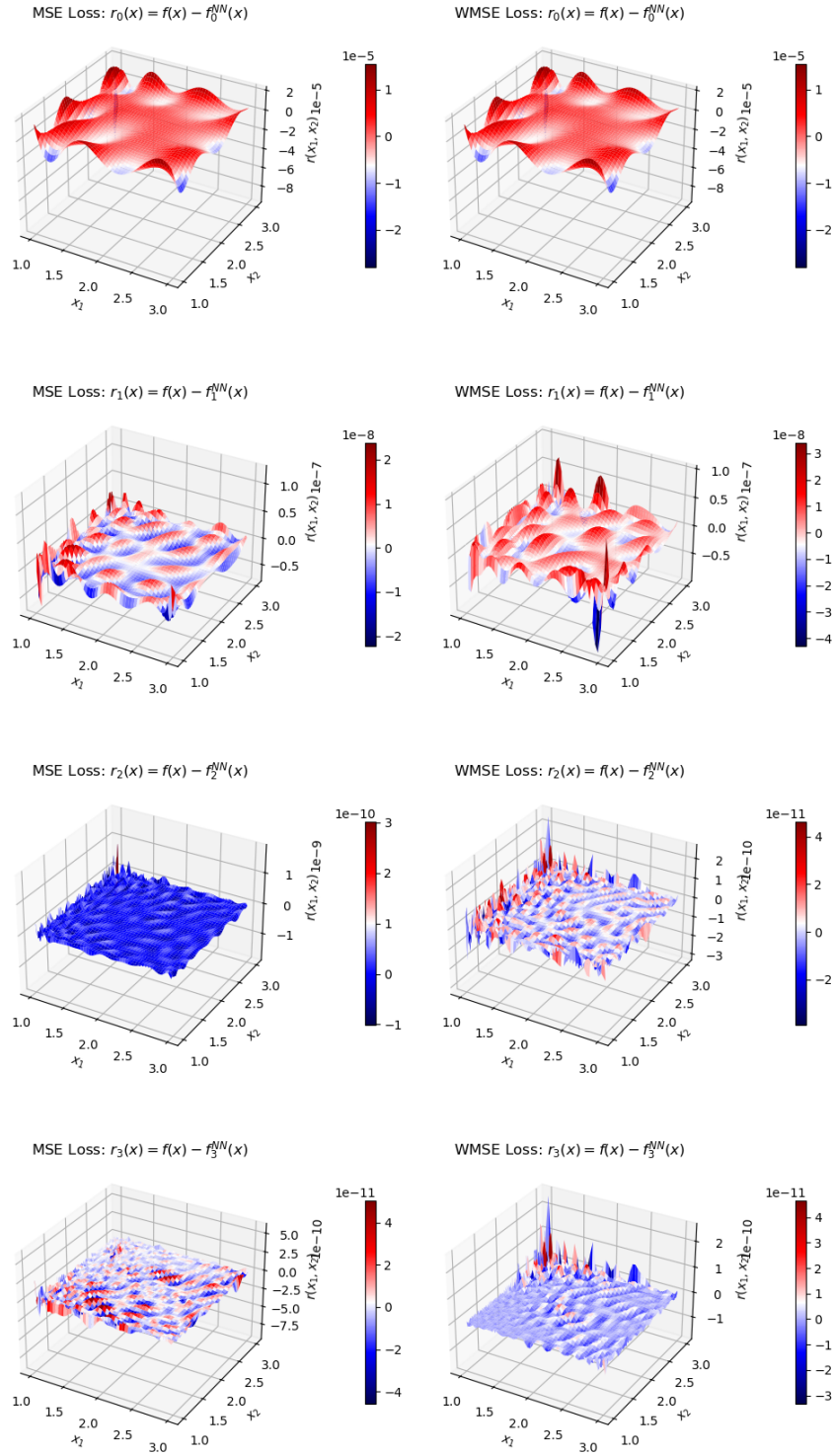


Figure 8: Comparison of residual predictions at each stage for Function I.6.2 using MSE loss (left column) and WMSE loss (right column), both with a [5-10-15-20] configuration. Note that the axis and colorbar scales between neighboring plots may differ to accurately illustrate the loss landscape from each approach.

does not increase the overall dataset size, maintaining computational requirements. Algorithm 2 revises Algorithm 1 to incorporate this method.

Algorithm 2 HiPreNet Training Algorithm with Weighted Sampling

Require: Dataset $(\mathbf{x}, \mathbf{f}) = \{(x_k, f(x_k))\}_{k=1}^N$, trained neural network f_0^{NN} , tolerance tol

$error \leftarrow L(\mathbf{f}, f_0^{NN}(\mathbf{x}))$
 $r_0 \leftarrow \mathbf{f} - f_0^{NN}(\mathbf{x})$
 $e_0 \leftarrow \max |r_0|$ ▷ estimate of true e_0
 $\hat{r}_0(\mathbf{x}) \leftarrow \frac{r_0}{e_0}$
 $p_0(\mathbf{x}) \leftarrow \frac{|\hat{r}_0(\mathbf{x})|}{\sum_{j=1}^N |\hat{r}_0(x_j)|}$
 $(\mathbf{x}_{sampled}, \hat{r}_0(\mathbf{x}_{sampled})) \leftarrow sample(p_0(\mathbf{x}))$
 $\hat{r}_0^{NN}(\mathbf{x}) \leftarrow train(\mathbf{x}_{sampled}, \hat{r}_0(\mathbf{x}_{sampled}))$
 $i \leftarrow 1$
while $error > tol$ **do**
 $f_i^{NN}(\mathbf{x}) \leftarrow f_i^{NN} + e_{i-1} \hat{r}_{i-1}^{NN}(\mathbf{x})$
 $r_i(\mathbf{x}) \leftarrow \mathbf{f} - f_i^{NN}(\mathbf{x})$
 $e_i \leftarrow e_{i-1} \cdot \max |r_i(\mathbf{x})|$ ▷ estimate of true e_i
 $\hat{r}_i(\mathbf{x}) \leftarrow \frac{r_i(\mathbf{x})}{e_i}$
 $p_i(\mathbf{x}) \leftarrow \frac{|\hat{r}_i(\mathbf{x})|}{\sum_{j=1}^N |\hat{r}_i(x_j)|}$
 $(\mathbf{x}_{sampled}, \hat{r}_i(\mathbf{x}_{sampled})) \leftarrow sample(p_i(\mathbf{x}))$
 $\hat{r}_i^{NN}(\mathbf{x}) \leftarrow train(\mathbf{x}_{sampled}, \hat{r}_i(\mathbf{x}_{sampled}))$
 $error \leftarrow L(\mathbf{f}, f_i^{NN}(\mathbf{x}))$
 $i \leftarrow i + 1$
end while

To evaluate the method, we applied weighted sampling across all five benchmark functions from the Feynman dataset using four-stage HiPreNets with widths [5–10–15–20], averaging across three simulations with different random seeds. A weighted resampling of the dataset before training each refinement networks focuses them on handling more challenging regions of the dataset without increasing dataset size, offering a computationally efficient route to reducing error. The sampling strategy generally maintains good overall coverage of the domain while prioritizing regions with higher residual error. In particular, samples near the boundaries of the domain, where the residuals tend to be largest, are selected more frequently during training. This suggests that the weighted sampling method effectively concentrates training effort on the areas that are most difficult to approximate, without requiring an increase in dataset size.

The final validation RMSE and L_∞ norm error for each function are given in Table 7, where we see that using weighted sampling with MSE loss gives the lowest RMSE and L^∞ norm error for all functions except for I.29.16. The best results for each function from Tables 6 where no weighted sampling was used and 7 where weighted sampling was used are compared in bar charts in Figure 9. We see that for four out of the five functions, weighted sampling successfully reduces both types of error.

To summarize, this method can lead to a noticeable reduction in both RMSE and L^∞ norm error. Similar to what was observed for the weighted mean square error loss function, weighted sampling does not guarantee a reduction in either error metric. It may cause the models to overfit to the training data, reducing their ability to generalize and worsening their performance on the validation data.

6 Targeted Model Correction with Local Residual Patching

In many real-world applications, models perform well on average but struggle with edge cases. For example, in medical diagnosis, a model may mispredict outcomes for patients with rare conditions, while in autonomous driving, unusual visual scenarios can lead to high prediction errors. For the functions we attempt to learn here, these edge cases are often along the boundary of the input domain. To address these challenges, we introduce a local patching technique that selectively refines model predictions in regions where performance is weakest.

Function	Loss	Final RMSE	Final L^∞ Norm Error
I.6.2	MSE	2.675e-12	8.111e-11
	WMSE	1.352e-11	3.830e-10
I.9.18	MSE	1.429e-07	8.714e-05
	WMSE	1.730e-07	1.201e-04
I.13.12	MSE	3.169e-07	2.473e-04
	WMSE	5.824e-07	4.729e-04
I.26.2	MSE	3.376e-06	2.018e-03
	WMSE	7.085e-06	3.900e-03
I.29.16	MSE	1.544e-05	3.555e-03
	WMSE	7.640e-06	8.989e-04

Table 7: The final validation RMSE and L^∞ norm error for both MSE and WMSE loss functions using the weighted sampling technique.

In this approach, once the HiPreNet algorithm is complete after m iterations, we evaluate the ensemble’s performance on a randomly selected set of validation points. We then identify the validation point x_{max} with the largest absolute prediction error.

$$x_{max} = \arg \max_{\mathbf{x}} |f(\mathbf{x}) - f_m^{NN}(\mathbf{x})|$$

Around this point, we define a neighborhood $N(x_{max})$ by selecting all points x within a specified radius r such that

$$N(x_{max}) = \{x \in \mathbf{x}, \|x - x_{max}\|_2 \leq r\}$$

Choosing the value for this radius is currently done manually, which does introduce a challenge in balancing there being enough data to train the localized network on versus introducing overfitting to a localized region of the domain.

These nearby points have their associated residuals $r_m(N(x_{max}))$ normalized according to

$$\hat{r}_m(x_{max}) = \frac{r_m(N(x_{max}))}{\max |r_m(N(x_{max}))|}$$

and form the training set for a new neural network $f_{patch}(x)$, specifically designed to model the behavior within this localized high-error region. After training, this network serves as a targeted “patching network” that refines the ensemble’s predictions by learning the normalized residuals in the identified area of weakness. The final prediction is now given by

$$f_{m+1}^{NN}(\mathbf{x}) = f_m^{NN}(\mathbf{x}) + \mathbb{1}(\mathbf{x})f_{patch}(\mathbf{x})$$

$$\mathbb{1}(\mathbf{x}) = \begin{cases} 1 & \text{for } x \in N(x_{max}) \\ 0 & \end{cases}$$

As an example, we consider Function I.13.12. From the left plot in Figure 10, the maximum validation error after training a 5-10-15-20 residual ensemble is located at the peak in the lower right corner of the domain. The sample at this peak is chosen, as well as all samples in a radius of $r = 0.75$ around it. A fully connected network with two hidden layers of 16 neurons each is then trained to learn the normalized residuals of these samples. After training this network, it is used to “patch” the region of the domain spanned by these samples. For any input to the final model, if it falls within this region, the patching network will be used and its prediction will be added to the final output. We then generate 1000000 new test data samples to test the generalization capabilities of this patching approach.

The RMSE and L^∞ norm errors on the validation data and test data from before and after the patching network is applied are given in Table 8. The final validation data residuals after patching are shown in the

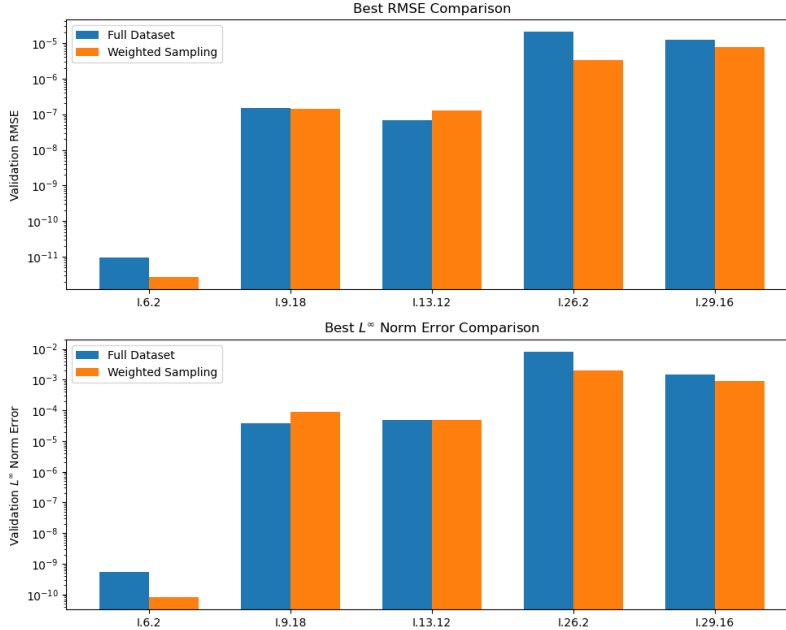


Figure 9: Bar chart showing the best validation RMSE and L^∞ norm error from Table 6 versus Table 7 for each function. To choose the best results, we choose the MSE or WMSE results based on which resulted in the lowest RMSE and lowest L^∞ norm error for that given function. Table 6 uses the full dataset to train each refinement network, while Table 7 uses the weighted sampling technique to train each refinement network.

right plot in Figure 10, and the final test data residuals before and after patching are given in Figure 11. As shown, by applying this patching approach, both the RMSE and the L^∞ norm error can be reduced by nearly an order of magnitude.

Data	Initial RMSE	Initial L^∞ Norm Error	Patching RMSE	Patching L^∞ Norm Error
I.13.12 Validation	1.399e-07	1.116e-04	3.284e-08	2.270e-05
I.13.12 Test	2.396e-07	2.325e-04	3.934e-08	3.419e-05

Table 8: Effect of applying local patching on Function I.13.12 with a comparison of validation RMSE and L^∞ norm error before and after patching.

By targeting the specific area around the worst-performing validation point, the patching network provides a focused correction that improves both RMSE and the L^∞ norm error. This technique demonstrates a scalable strategy for enhancing model reliability in applications where global accuracy masks localized weaknesses.

7 Improving Boundary Accuracy through Domain Expansion

The largest errors in training neural network models often occur along the boundary of the training domain. To address this issue, we propose training the neural network on an input domain that is larger than the domain of interest. This technique allows the neural network to better approximate the boundary in the true evaluation domain, reducing the overall RMSE and L^∞ norm error. In practice, this technique could be used for applications such as material science and manufacturing, where training data can be collected for features such as temperature and strain that is outside the expected domain in operation, but can still be collected in practice.

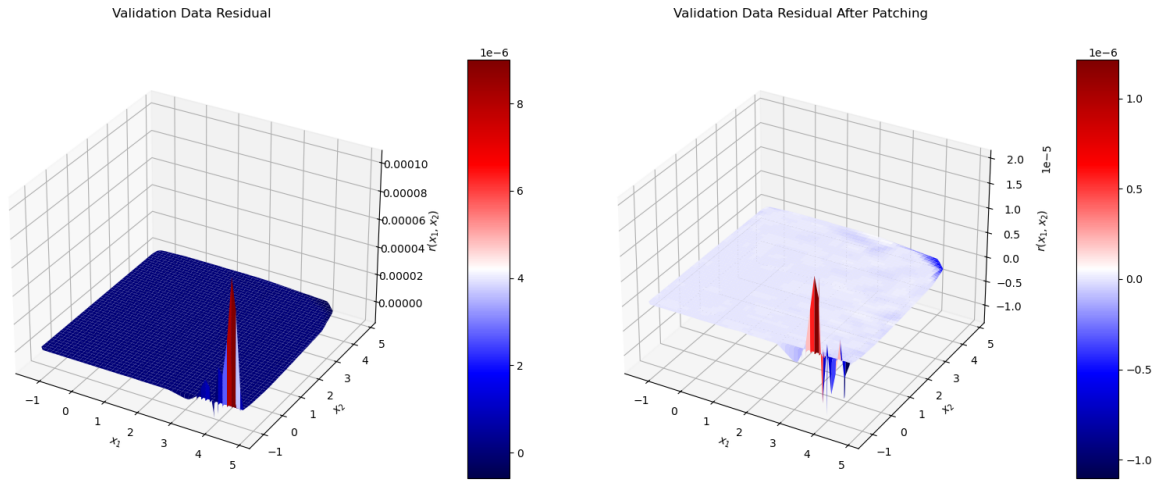


Figure 10: Validation data residuals for Function I.13.12: the left plot shows final residuals after standard HiPreNet training and the right plot includes the correction from a localized patching network.

Let $f(x) : D \rightarrow R$ be a continuous function defined on compact domain $D \subset R^n$. We approximate f with a neural network $f^{NN}(x)$ by training it on a larger domain $\hat{D} \supset D$. This approach aims to mitigate boundary-related errors by allowing the network to learn beyond the boundary, thereby improving its robustness and performance on the target domain D .

We evaluate this approach on Function I.13.12, where 1,000,000 validation samples are generated with all input variables in $[1.1, 4.9]$. Two residual ensembles are trained: one on 1,000,000 samples from the domain $[1.1, 4.9]$ (the baseline), and another on the slightly expanded domain $[1, 5]$. We compare each ensemble’s performance on the validation data in Table 9 and in Figure 12, where we see that the ensemble trained on an expanded domain sees a substantial reduction in RMSE and L^∞ norm error.

Function	Training Domain	Final RMSE on [1.1,4.9]	Final L^∞ Norm Error on [1.1,4.9]
I.13.12	[1,5]	6.061e-08	2.569e-06
	[1.1,4.9]	3.523e-07	1.121e-04

Table 9: The final validation RMSE and L^∞ norm error for evaluating on data in $[1.1,4.9]$ for one network trained on data in $[1,5]$ and another trained on data in $[1.1,4.9]$. Averaged across three trials.

To explore the limits of this approach, we conduct a second experiment with a more pronounced domain expansion. Now, the 1,000,000 validation data samples are all generated to have input variables in $[2, 4]$. Again, two residual ensembles are trained with 1,000,000 samples: one on $[2, 4]$ and the other on the same expanded domain $[1, 5]$. The final RMSE and L^∞ norm error for each ensemble is given in Table 10. We now observe that the expanded domain ensemble performs noticeably worse in RMSE than the original domain

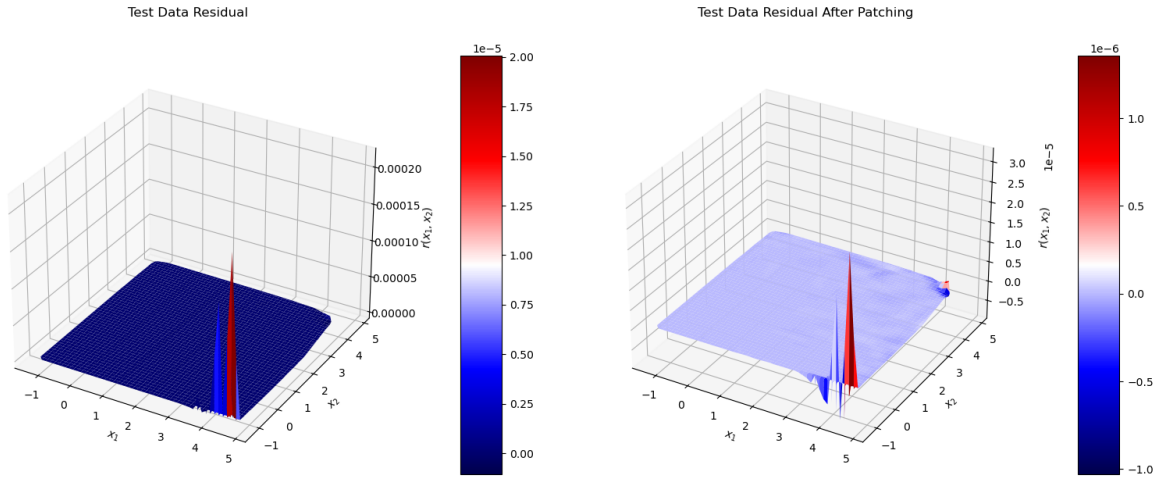


Figure 11: Test data residuals for Function I.13.12: the left plot shows final residuals after standard HiPreNet training and the right plot includes the correction from a localized patching network.

ensemble. This suggests that when the expanded region is too large relative to the target domain, the model may underfit the region of interest unless given a proportionally larger training set.

Function	Training Domain	Final RMSE on [2,4]	Final L^∞ Norm Error on [2,4]
I.13.12	[1,5]	2.728e-08	1.279e-07
	[2,4]	1.883e-10	1.057e-07

Table 10: The final validation RMSE and L^∞ norm error for evaluating on data in [2,4] for one network trained on data in [1,5] and another trained on data in [2,4]. Averaged over three trials.

In summary, expanding the training domain can significantly reduce boundary errors when the expanded region is modest and representative. However, overly broad expansion may lead to underfitting in the target domain unless training density is increased or weighted sampling is applied. This approach could potentially be expanded to applications where it is not possible to collect data outside the target domain. For example, in climate prediction models, it may be beneficial to extrapolate existing data beyond its limits to include some “unfeasible” cases.

8 Conclusion

Training highly accurate neural networks for scientific and engineering tasks remains challenging due to the complex interplay of non-convex optimization, sensitivity to hyperparameters, and the lack of a structured framework for improving worst-case error. Inspired by the principles of gradient boosting from classical

Equation I.13.12

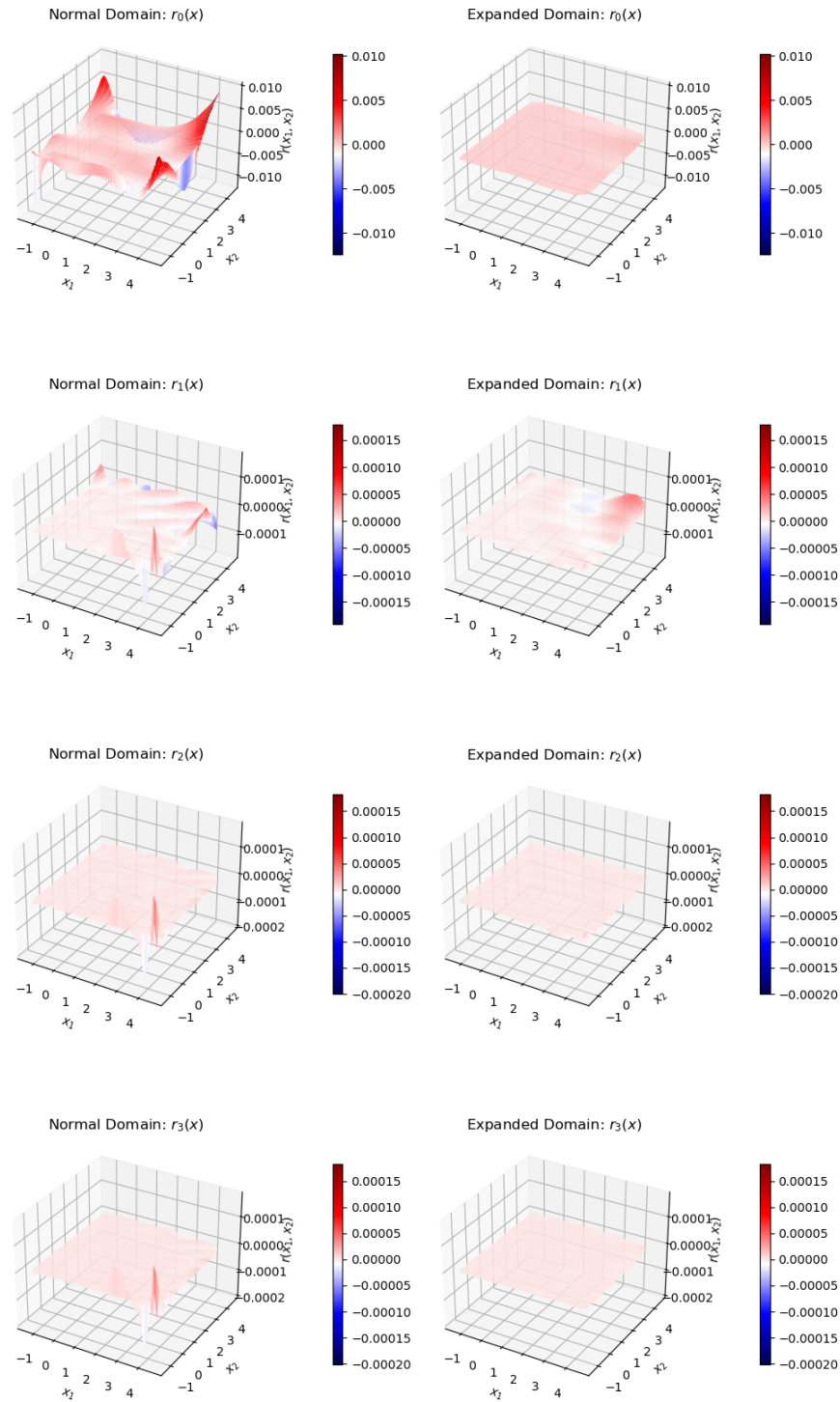


Figure 12: Validation results on data generated in [1.1, 4.9] at each iteration. The normal domain network is trained on data generated in [1.1, 4.9], while the expanded domain network is trained on data generated in [1, 5].

Equation I.13.12

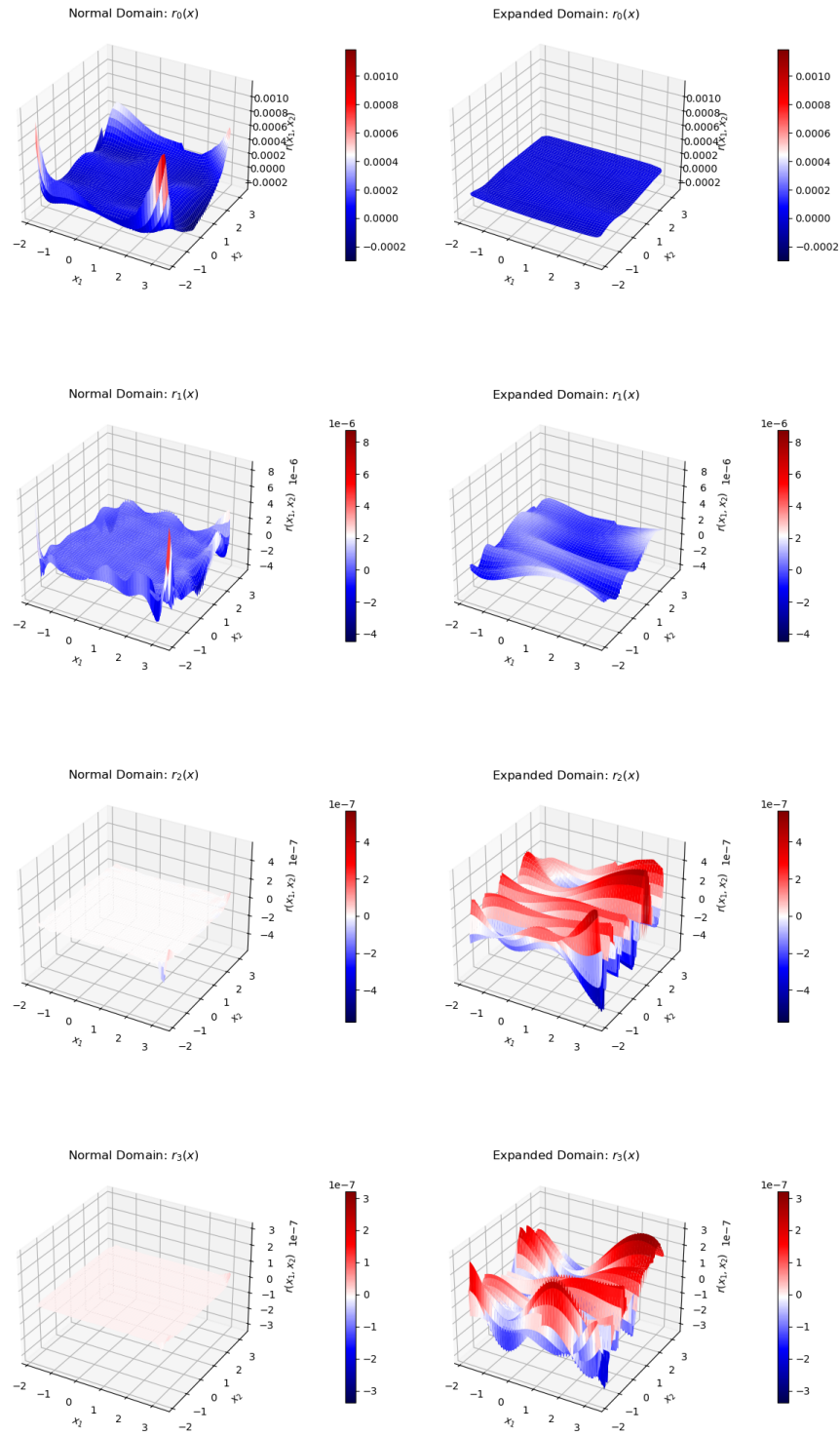


Figure 13: Validation results on data generated in [2, 4] at each iteration. The normal domain network is trained on data generated in [2, 4], while the expanded domain network is trained on data generated in [1, 5].

machine learning, our approach decomposes the problem of fitting a complex function into a sequence of simpler tasks, where each stage of training focuses on correcting the residual errors of its predecessor. This method not only reduces the dependence on extensive hyperparameter tuning, but also offers a modular and more scalable path toward model refinement.

Unlike traditional approaches that rely heavily on minimizing average error via mean squared loss, our method also prioritizes control over the L^∞ norm error, which is crucial in domains that require safety-critical decision-making. Through extensive experiments on regression problems drawn from the Feynman dataset, we demonstrated that our HiPreNet framework consistently improves both RMSE and L^∞ norm error, outperforming standard fully connected networks and even more advanced architectures like Kolmogorov–Arnold Networks (KANs).

We further explored design strategies that enhance this framework to further reduce both the RMSE and L^∞ norm error, such as adaptively increasing network width across residual stages, using loss functions targeted at maximum error reduction, and applying targeted techniques such as local patching and training domain expansion to focus on correcting regions of greatest error. These strategies do not always offer guaranteed improvement, but offer additional ways to approach the design of a HiPreNet framework that may be suitable for a given task.

In future work, it would be worthwhile to explore if there are certain properties of the residuals that can be taken advantage of to determine the optimal size of each refinement network. It would additionally be worthwhile to modify the framework to handle tasks such as time series data or classification. The HiPreNet framework can also be extended to more complex architectures such as convolutional neural networks or physics informed neural networks, enabling improved performance on computer vision problems or data governed by physical laws.

References

- [1] S. Abrecht, A. Hirsch, S. Raafatnia, and M. Woehrle. Deep learning safety concerns in automated driving perception. *IEEE Transactions on Intelligent Vehicles*, 2024.
- [2] D. Amodei, C. Olah, J. Steinhardt, P. Christiano, J. Schulman, and D. Mané. Concrete problems in ai safety. *arXiv preprint arXiv:1606.06565*, 2016.
- [3] V. Antun, F. Renna, C. Poon, B. Adcock, and A. C. Hansen. On instabilities of deep learning in image reconstruction and the potential costs of ai. *Proceedings of the National Academy of Sciences*, 117(48):30088–30095, 2020.
- [4] S. Badirli, X. Liu, Z. Xing, A. Bhowmik, K. Doan, and S. S. Keerthi. Gradient boosting neural networks: Grownet. *arXiv preprint arXiv:2002.07971*, 2020.
- [5] Y. Bengio. Gradient-based optimization of hyperparameters. *Neural computation*, 12(8):1889–1900, 2000.
- [6] L. Breiman, J. H. Friedman, R. A. Olshen, and C. J. Stone. Classification and regression trees. 1984.
- [7] T. Chen and C. Guestrin. Xgboost: A scalable tree boosting system. In *Proceedings of the 22nd acm sigkdd international conference on knowledge discovery and data mining*, pages 785–794, 2016.
- [8] A. Choromanska, M. Henaff, M. Mathieu, G. B. Arous, and Y. LeCun. The loss surfaces of multilayer networks. In *Artificial intelligence and statistics*, pages 192–204. PMLR, 2015.
- [9] V. G. Costa and C. E. Pedreira. Recent advances in decision trees: An updated survey. *Artificial Intelligence Review*, 56(5):4765–4800, 2023.
- [10] Y. N. Dauphin, R. Pascanu, C. Gulcehre, K. Cho, S. Ganguli, and Y. Bengio. Identifying and attacking the saddle point problem in high-dimensional non-convex optimization. *Advances in neural information processing systems*, 27, 2014.

- [11] C. Dong, L. Zheng, and W. Chen. Kolmogorov-arnold networks (kan) for time series classification and robust analysis. In *Advanced Data Mining and Applications: 20th International Conference, ADMA 2024, Sydney, NSW, Australia, December 3–5, 2024, Proceedings, Part IV*, page 342–355, Berlin, Heidelberg, 2024. Springer-Verlag.
- [12] J. H. Friedman. Greedy function approximation: a gradient boosting machine. *Annals of statistics*, pages 1189–1232, 2001.
- [13] Q. Gong, W. Kang, and F. Fahroo. Approximation of compositional functions with relu neural networks. *Systems & Control Letters*, 175:105508, 2023.
- [14] I. Goodfellow, J. Shlens, and C. Szegedy. Explaining and harnessing adversarial examples. In *International Conference on Learning Representations*, 2015.
- [15] K. Hornik, M. Stinchcombe, and H. White. Multilayer feedforward networks are universal approximators. *Neural networks*, 2(5):359–366, 1989.
- [16] W. Kang and Q. Gong. Feedforward neural networks and compositional functions with applications to dynamical systems. *SIAM Journal on Control and Optimization*, 60(2):786–813, 2022.
- [17] A. N. Kolmogorov. On the representation of continuous functions of several variables by superpositions of continuous functions of one variable and addition. *Doklady Akademii Nauk SSSR*, 114:953–956, 1957.
- [18] A. Krizhevsky, I. Sutskever, and G. E. Hinton. Imagenet classification with deep convolutional neural networks. *Advances in neural information processing systems*, 25, 2012.
- [19] Z. Liu, Y. Wang, S. Vaidya, F. Ruehle, J. Halverson, M. Soljacic, T. Y. Hou, and M. Tegmark. KAN: Kolmogorov–arnold networks. In *The Thirteenth International Conference on Learning Representations*, 2025.
- [20] E. J. Michaud, Z. Liu, and M. Tegmark. Precision machine learning. *Entropy*, 25(1):175, 2023.
- [21] J. Nocedal and S. Wright. *Numerical Optimization*. Springer Science & Business Media, 2nd edition, 2006.
- [22] J. R. Quinlan. Induction of decision trees. *Machine learning*, 1:81–106, 1986.
- [23] J. R. Quinlan. *C4.5: Programs for Machine Learning*. Morgan Kaufmann Publishers Inc., San Francisco, CA, USA, 1993.
- [24] A. Radford, K. Narasimhan, T. Salimans, I. Sutskever, et al. Improving language understanding by generative pre-training. 2018.
- [25] N. Rahaman, A. Baratin, D. Arpit, F. Draxler, M. Lin, F. Hamprecht, Y. Bengio, and A. Courville. On the spectral bias of neural networks. In *International conference on machine learning*, pages 5301–5310. PMLR, 2019.
- [26] F. Rosenblatt. The perceptron: A perceiving and recognizing automaton. Report, Project PARA, Cornell Aeronautical Laboratory, Jan. 1957.
- [27] D. E. Rumelhart, G. E. Hinton, and R. J. Williams. Learning representations by back-propagating errors. *nature*, 323(6088):533–536, 1986.
- [28] J. Snoek, H. Larochelle, and R. P. Adams. Practical bayesian optimization of machine learning algorithms. *Advances in neural information processing systems*, 25, 2012.
- [29] M. Tan and Q. Le. Efficientnet: Rethinking model scaling for convolutional neural networks. In *International conference on machine learning*, pages 6105–6114. PMLR, 2019.
- [30] S.-M. Udrescu and M. Tegmark. Ai feynman: A physics-inspired method for symbolic regression. *Science Advances*, 6(16):eaay2631, 2020.

- [31] A. Vaswani, N. Shazeer, N. Parmar, J. Uszkoreit, L. Jones, A. N. Gomez, L. u. Kaiser, and I. Polosukhin. Attention is all you need. In I. Guyon, U. V. Luxburg, S. Bengio, H. Wallach, R. Fergus, S. Vishwanathan, and R. Garnett, editors, *Advances in Neural Information Processing Systems*, volume 30. Curran Associates, Inc., 2017.
- [32] P. Virtanen, R. Gommers, T. E. Oliphant, M. Haberland, T. Reddy, D. Cournapeau, E. Burovski, P. Peterson, W. Weckesser, J. Bright, S. J. van der Walt, M. Brett, J. Wilson, K. J. Millman, N. Mayorov, A. R. J. Nelson, E. Jones, R. Kern, E. Larson, C. J. Carey, Í. Polat, Y. Feng, E. W. Moore, J. VanderPlas, D. Laxalde, J. Perktold, R. Cimrman, I. Henriksen, E. A. Quintero, C. R. Harris, A. M. Archibald, A. H. Ribeiro, F. Pedregosa, P. van Mulbregt, and SciPy 1.0 Contributors. SciPy 1.0: Fundamental Algorithms for Scientific Computing in Python. *Nature Methods*, 17:261–272, 2020.
- [33] Y. Wang and C.-Y. Lai. Multi-stage neural networks: Function approximator of machine precision. *Journal of Computational Physics*, 504:112865, 2024.
- [34] S. Xie, R. Girshick, P. Dollár, Z. Tu, and K. He. Aggregated residual transformations for deep neural networks. In *Proceedings of the IEEE conference on computer vision and pattern recognition*, pages 1492–1500, 2017.
- [35] C. Zhang, S. Bengio, M. Hardt, B. Recht, and O. Vinyals. Understanding deep learning (still) requires rethinking generalization. *Commun. ACM*, 64(3):107–115, Feb. 2021.